10

Numerical Wave Flumes Based on Smoothed Particle Hydrodynamics

Jinhai Zheng[1*], Gang Wang[1], Chi Zhang[2] and Yingqi Liu[2]
[1]*State Key Laboratory of Hydrology-Water Resources and Hydraulic Engineering, Hohai University, Nanjing,*
[2]*College of Harbour, Coastal and Offshore Engineering, Hohai University, Nanjing, China*

1. Introduction

Numerical simulation using computers or computational simulation has increasingly become a very important approach for solving complex practical problems in engineering and science. It translates a physical problem into a discrete set of mathematical description, recreates and solves the problem on a computer, and reveals phenomena virtually according to the requirements of the analysts. With the help of increasing computer power less and less assumptions are necessary and problems can be solved with more details. Numerical simulations are replacing expensive, time-consuming and difficult experiments in laboratories more and more. Furthermore, the numerical tools are often more useful than the traditional experimental methods in terms of providing insightful and complete information that cannot be directly measured or observed, or difficult to acquire via other means.

Hydraulic engineering is defined as the branch of civil engineering dealing with the use and control of water in motion. Numerical simulation is an important tool to understand the motion of water. For fluid motion, it can be described by a set of partial differential equations in time and space. Pressure, and a velocity component for every used dimension, is the only main independent field variables. With enough initial and boundary conditions the equations can be solved giving the pressure and velocity at every point, at every time. In most cases analytical solutions are not available. However, when space is discretized into cells (regular or irregular), and time is divided in a finite number of steps, the solution can be found by numerical integration. There are many ways to discretize the continuous governing equations, and the discretization techniques may be different for different numerical methods.

Traditional numerical methods, such as the finite difference method, the finite volume method and the finite element method, are based on Eulerian grids, which is that the grid is fixed and the fluid is flowing through it. The finite difference method uses a fixed rectangular grid and discretizes the equations using Taylor Series expansion. This method

*Corresponding author

was used historically due to its ease of programming and accurate results but tends to rely on a fairly regular mesh. It therefore does not handle large deformations or complex problems well. Recently, the method discretized the equations in generalized curvilinear coordinates has also been developed to adapt computations to irregularly shaped boundaries and make computations more efficient. The finite volume method discretizes the domain into a number of finite volumes and integrates the governing equations over each of these. This method is popular amongst fluid dynamics researchers because integrals are applied separately within each volume. One applies the conservation principle (volume integration) and exploits the Gauss Green theorem to turn a volume problem into a surface one; the rate of change of one property inside a control volume can now be assessed by the computation of the property fluxes at the boundaries. A structured grid is not required when using this method giving it an advantage due to the effort saved. The finite element method divides the domain up into elements (usually in the form of basic geometric shapes, such as triangular grids). The numerical solution is also determined by integration albeit a weighed integration and shape functions are also used to express the value of a property continuously as a combination of the cell nodal values. An attractive feature of the finite element method is that it is well suited to handling complicated geometries and generally considered to be very robust.

Despite these conventional grid-based numerical methods have got the great success in computational fluid dynamics for engineering and science problems, they suffer from some inherent difficulties in many aspects, which limit their applications to many problems. One drawback is capturing the position of the free surface, and it is difficult to predict when it changes rapidly in time. A multiply defined free surface as in overtopping waves is harder or even impossible to predict for these methods.

Smoothed Particle Hydrodynamics (SPH) is a pure Lagrangian, meshfree method, which was conceived in 1977 by Gingold and Monaghan[1] and independently by Lucy[2] for modeling astrophysical phenomena, and later widely extended for applications to problems of continuum solid and fluid mechanics. The basic idea of SPH is to use the collective motions of large number of particles to represent a flow in a Lagrangian way rather than Eulerian way. In a particle approach, the governing equations are discretized and solved with respect to the individual particles filled within the computational domain. This method is conceptually simple without adding new physics and high accuracy can be achieved by increasing number of particles.

To date, the SPH becomes increasingly popular and finds wide applications in computational fluid mechanics, including free surface flow[3], porous flow[4], landslide-induced flow[5] and fluid-structure interactions[6]. In particular, the SPH method has been adapted in a variety of numerical wave flumes for studying green water overtopping[7-8], wave breaking in the surf zone[9-10], and wave-structure interaction[11-13]. The most attracting feature of SPH for wave modeling is that it naturally needs no special approach for dealing with the free surface. It is meshfree and every particle at the free surface can be easily tracked in the Lagrangian frame. When conducting a numerical wave flume involved with flow separation and large deformation, this appears a significant advantage over other traditional Eulerian methods, including those based on the Reynolds Averaged Navier-Stokes (RANS) equations[14], large eddy simulation[15-16], and Laplace models[17]. Those models commonly need an additional treatment to capture the free surface on a fixed

Eulerian grid, such as the Volume Of Fluid (VOF) method or the MAC method. Moreover, those Eulerian solvers often suffer from the numerical diffusion arising from the fixed-point interpolations of advection terms. In the Lagrangian description of SPH simulations, this problem is avoided. Besides, the SPH can handle rotational flows with vortices and turbulence.

Despite its remarkable advances for simulation of violent free-surface fluid flows, the most critical drawback of SPH which limits the future applications is its extreme demand for CPU time. As was pointed out by Dalrymple and Rogers[9], the SPH method is not suitable to model large regions at the present state of art, since a large number of particles and rather small time step are often required to obtain satisfactory resolution. One of the most important factors resulting in the long CPU time is a searching process for the nearest neighboring particles for every given particle, which should be updated at each time step, called the Nearest Neighboring Particle Search (NNPS). The efficiency of NNPS method thus dominates the overall computational cost. The earliest and simplest NNPS method is the Direct Search Method (DSM), which directly computes the distances between each pair of particles to find the smallest one. Clearly, the computation order would be $O(N^2)$ (where N is the total number of particles) for this method. A variety of improvements have been made to decrease the count of operations in this process. Monaghan[18] proposed the Link-List Method (LLM), which divides all particles into rectangle grids. When searching the nearest particles of a certain particle, only those within the same grid as this one and within 8 adjacent grids around are taken into consideration. However, this method behaves poor if the density of particles is largely non-uniform over the whole domain. Hernquist and Katz[19] developed a hierarchical tree method which reduced the computation order to $O(N \cdot \log N)$. Mihai et al.[20] used a static grid system with variable spatial steps and successfully decreased the computation order to $O(N)$. Those improvements are, however, still far away from satisfactory, regarding the considerably increasing number of particles needed in wider applications of SPH method. Recently, Zheng et al.[21] proposed a new NNPS method, named as the Inner and Outer Particles Searching (IOPS) method. The method distinguishes itself from others by introducing concepts of inner and outer grids, which significantly enhances the computation efficiency compared with the DSM and the method of Mihai et al.[20].

In this paper, section 2 introduces the development of a SPH numerical wave flume based on the Navier-Stokes equations, following by a description of the IOPS method that enhances the SPH method. Section 3 validates the numerical results, which are compared with the analytical solutions, other methods and experiment data. Section 4 applies the SPH method for a wide range of solitary wave propagation problems such as the impact of waves on structures, wave run-up and rundown and breaking on a planar slope. Finally in section 5, conclusions about SPH are drawn and further improvements are recommended.

2. Numerical method

The basic concept of SPH method is to treat a flow as a sum of moving particles. Each particle has its own physical quantities such as mass, velocity, density and pressure gradient. During flow motions, all particles change their positions and corresponding properties with time. The SPH model then solves the trajectory of each particle. Through the

use of integral interpolations, the field variables are expressed by integrals approximated by summation interpolations over neighboring particles. Firstly, the functions of variables at an arbitrary location are transformed into integral forms, referred to the kernel approximation. Secondly, those integral expressions are approximated by summations of variables of relevant scattered particles.

2.1 Kernel approximation

In a continuous variable field, any function can be expressed in terms of its values at a set of particles by use of a weighting function

$$A(r)=\int_{\Omega} A(r')\delta(r-r')\mathrm{d}r' \tag{1.1}$$

and

$$\delta(r-r')=\begin{cases}1, & r=r'\\ 0, & r\neq r'\end{cases} \tag{1.2}$$

where A is the function with respect to the spatial tensor, Ω denotes the computational domain, and δ $(r - r')$ is Dirac delta function. Replacing the Dirac delta function by a kernel W, leads to

$$A(r)=\int_{\Omega} A(r')W(r-r',h)\mathrm{d}r' \tag{1.3}$$

where h is the smoothing length which controls the size of the area around a given particle where the contribution from other particles cannot be neglected, and W is a cubic spline kernel. Representing the approximation process with a sign of <> and introducing the gradient of $A(r)$, we get

$$\langle \nabla A(r)\rangle=\int_{\Omega}\left[\nabla A(r')\right]W(r-r',h)\mathrm{d}r' \tag{1.4}$$

Equation (1.4) can be written as

$$\langle \nabla A(r)\rangle\approx-\int_{\Omega} A(r')\nabla W(r-r',h)\mathrm{d}r' \tag{1.5}$$

provided that the filtering range kh is inside the computational domain Ω .

Note that, if the filtering range extends beyond the computational domain, Eq. (1.5) will break down for the lack of particles and a special treatment should be applied at the boundary[22].

2.2 Particle approximation

If the number of particles constructing the whole domain is N, Eq.(1.5) can be approximated

by a summation, given as

$$\langle \nabla A(r) \rangle \approx -\sum_{b=1}^{N} \frac{m_b}{\rho_b} A(r_b) \nabla W(r - r_b, h) \tag{1.6}$$

where r, m and ρ represent the spatial vector, mass and density of an individual particle, respectively. Subscript b represents the index number.

It can be seen from Eq.(1.6) that the variable A at the point r is affected by all N particles in the computation domain. In practice, the influence of kernel is restricted to a radial distance of an order of kh. That means only the particles within this distance (so-called neighboring particles) are considered to contribute to the summation in Eq.(1.6). While particles keep moving with flow motions, the relative positions of all particles should be calculated to find the effective particles for each point at every time step. This work is done by the NNPS method.

2.3 IOPS method

This section describes in detail the concept and implementation of the IOPS method proposed in this study. The IOPS method saves the computational time by shifting most of advanced CPU operations (e.g., multiplication, division) into simple addition operations. Firstly, each individual particle is marked by the so-called inner and outer grids. Secondly, for a given particle inside the domain, the particles in its filtering control unit in the inner grid is marked. Finally, the distances between this particle and other particles in the filtering control unit are computed to find the nearest neighboring particles.

If the number of particles is N and the number of inner grids is m for the whole domain, the number of particles in each inner grid would be N/m. Figure 1 shows the grid structures. Overlaps can be seen between boundaries of neighboring outer grids. The number of particles in each outer grid is larger than that in each inner grid. When total number of particles is relatively large, however, that difference can be neglected in the estimation of computational effort. Therefore, the computation order of marking all particles by inner and outer grids is $O(2\times N\times m)$.

For a given particle in an inner grid, a square filtering control unit is defined with its side length of kh. Then, particles belonging to both the filtering unit and the outer grid are marked, with a computation order of $O(N^2/m^2)$. For the whole domain, that is $O(N^2/m)$. Till now, only particles inside the filtering control unit need to be considered to search the nearest neighboring ones. The computation order for this process appears a constant and can no longer be reduced. Eventually, it is easy to find that the smallest total computation order can only be obtained when $2\times N\times m+N^2/m$ is smallest. That is when $m=\sqrt{N/2}$, we get the minimum CPU time consuming.

To highlight the efficiency of the IOPS method, the CPU time required for a single searching process using the present method, DSM and the method of Mihai et al.[20] are illustrated in Figure 2. The x-axis represents the total number of particles and the y-axis represents the CPU time. All numerical experiments in this paper were carried out on a PC with a CPU 1.83 GHz. An obvious advancement of IOPS over other two methods can be found, with a

computation order of $O(N)$. In particular, unlike those two methods, the good behavior of IOPS is not significantly affected by increasing number of particles even for extreme large values. For 205,000 particles, only a CPU time of 4.2 s is needed to complete a searching using the IOPS. This improvement releases the SPH applications for practical purposes to a considerable extent.

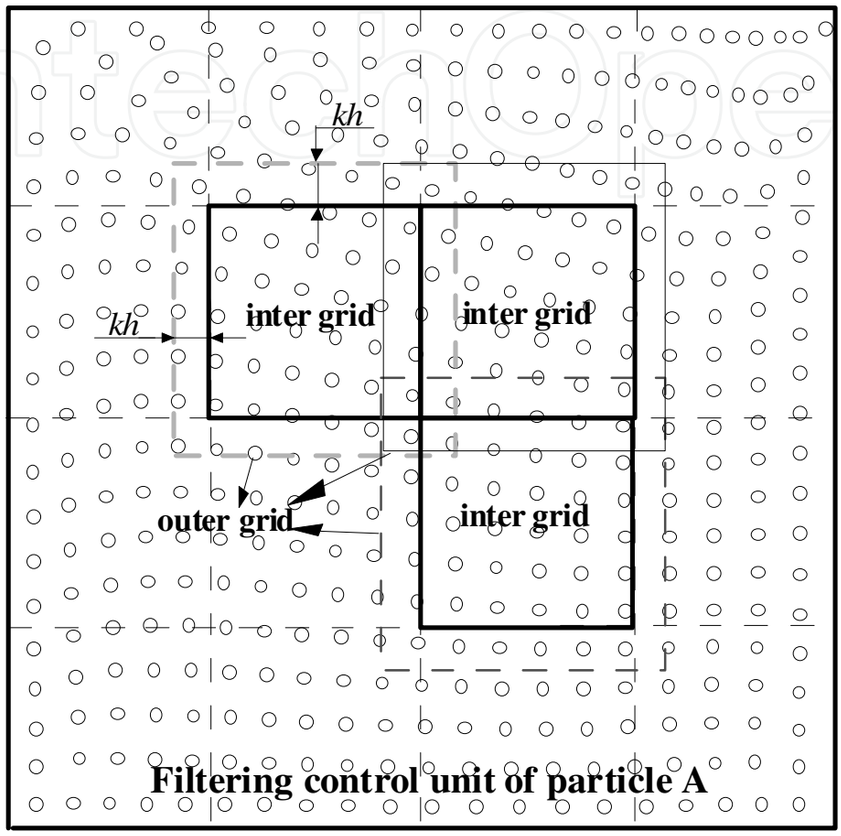

Fig. 1. Grid structure in the IOPS method

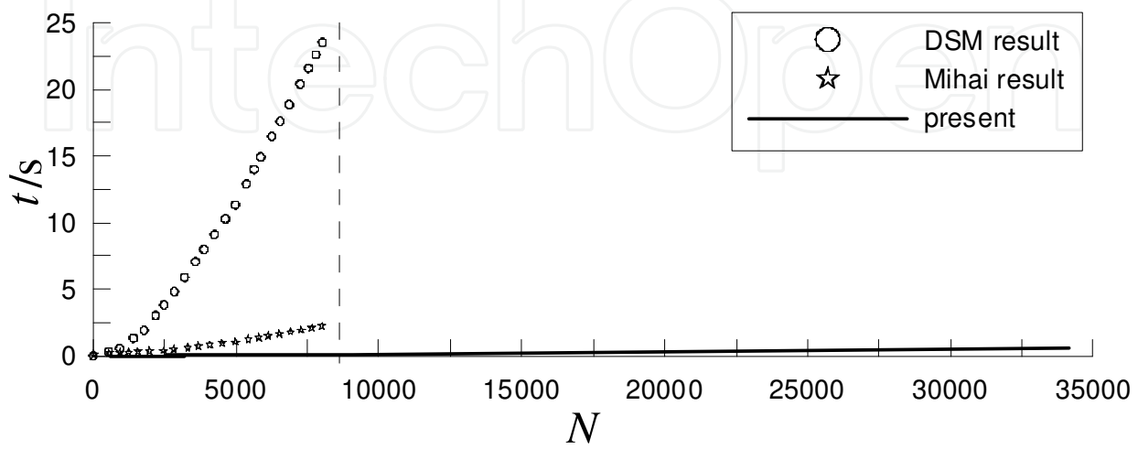

Fig. 2. Comparisons of CPU time required for a single searching by three NNPS methods

2.4 Numerical wave flume

In Lagrangian form, the conservation of mass and the conservation of momentum for a Newtonian incompressible fluid can be expressed as

$$\frac{\mathrm{d}\rho}{\mathrm{d}t} + \rho\nabla\cdot\mathrm{u} = 0 \tag{1.7}$$

$$\frac{\mathrm{du}}{\mathrm{d}t} = F - \frac{1}{\rho}\nabla p + \nu\nabla^2\mathrm{u} \tag{1.8}$$

where **u** is the particle velocity tensor, p the fluid pressure, ν the kinematic viscosity, F the body force per unit mass.

The pressure of each particle is obtained from the equation of state. By artificially enhancing the fluid compressibility, the following form is proposed

$$p = \frac{\rho_0 c_0^2}{\gamma}\left[\left(\frac{\rho}{\rho_0}\right)^{\gamma} - 1\right] \tag{1.9}$$

where ρ_0 is a reference density which is usually taken as the density of the fluid at the free surface, c_0 the speed of sound which is set much lower than its correct value to maintain numerical stability, γ the polytropic constant, usually set to be 7 for water.

At the free surface, the Dirichlet condition is applied according to Koshizukar et al.[23]. If the density calculated at particle a satisfies the following criterion

$$\rho_a < \beta\rho_0 \tag{1.10}$$

then the particle is regarded as a free-surface particle (constant β = 0.8 - 0.98) for which a density equal to ρ_0 is imposed. This treatment is based on the fact that the calculated particle density on the free surface drops abruptly for the lack of particles in the outer region of the free surface.

For the fixed solid boundary, a method involving fixed wall particles and mirror particles are used[24], as shown in Figure 3. Additional repulsive forces are imposed to wall particles to balance the pressure of inner fluid particles and prevent them from penetrating the wall. Several lines of mirror particles are placed on the outer side of the wall with their pressure setting equal to that of neighboring wall particles. The symmetrical nature of mirror particles ensures the pressure balance at the fixed boundary and makes the homogeneous Neumann condition applied.

3. Model results

3.1 Dam breaking

The study of the waves caused by the failure of a dam has attracted significant interest. This can be attributed to the significant consequences of dam failure particularly in cases where dams are located upstream of large conurbations, where the population has mostly grown

considerable since the dam's original construction. Along with the significance of the consequences, the challenges of adequately capturing the physics of the problem and the difficulty of solving the associated equations mathematically have attracted the attention of researchers. In the past similar simulations have been executed with the Marker-and-Cell method (MAC)[25] and the mesh-based Volume-of-Fluid method (VOF)[26]. These approaches have shown some benefits, but the resolution of the free surface is neither straightforward nor entirely accurate. Increased accuracy may be obtained using adaptive meshing, but at a significant cost. This style of dam failure has recently attracted the attention of researchers using SPH in particular, which is very suitable to describe this problem with a fast varying water level.

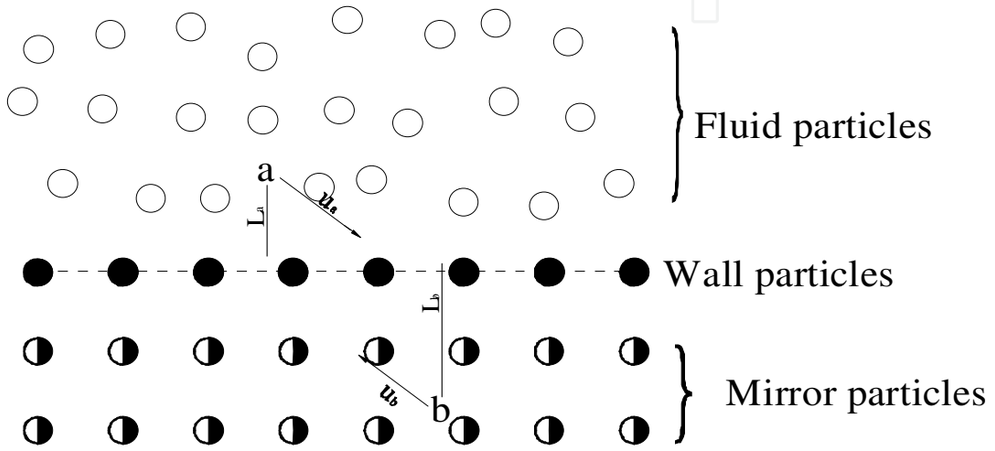

Fig. 3. Particle setting at the fixed solid boundary

A rectangular water column with a width of 0.1 m and a height of 0.2 m is confined between two vertical walls. At the beginning of the simulation, the right wall is instantaneously removed and the water is allowed to collapse due to gravity and flow out along the dry horizontal bed. In computation, a total number of N = 20× 40 of particles are configured, corresponding to an initial particle spacing of 0.005 m. A constant time step of 0.0005s is used. The kinematic viscosity is $\nu = 10^{-6}$ kg·ms^{-1}. A cubic spline kernel is employed and the smoothing length is 1.2 × 2 times of the initial particle spacing.

The particle snapshots of flow at different times t = 0.05s, t = 0.1s, t =0.15s, and t = 0.18s are shown in Figure 4. The fluid is firstly squeezed out at the bottom of the column, and then the top of the column moves down. The simulated free surfaces are consistent to those computed by Shao and Lo[27]. The leading edges of flow strictly follow the wall boundary at all moments, indicating that the pressure of fluid particles in the dry-wet transition region is correctly estimated. Figure 5 shows the position of leading edge $X = x / H$ versus the normalized time $T = t\sqrt{g/H}$ in the present simulation, as well as the results from experiments [27-28], the VOF method[26], and the MAC method[25]. Good agreements are found. The velocity field at t = 0.15s is illustrated in Figure 6. As is shown, the particle velocities in the water jet are relatively large due to strong pressure gradient, while those in the inner flow column remain almost static due to particle-particle interactions and the small pressure gradients there.

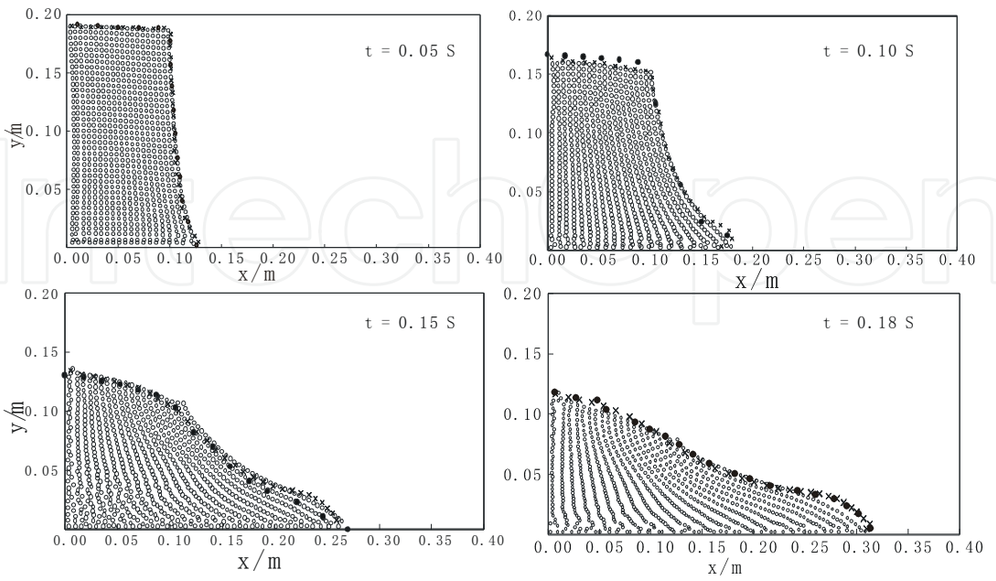

Fig. 4. Particle snapshots after dam breaking at t = 0.05s, t = 0.10s, t = 0.15s and t = 0.18s.

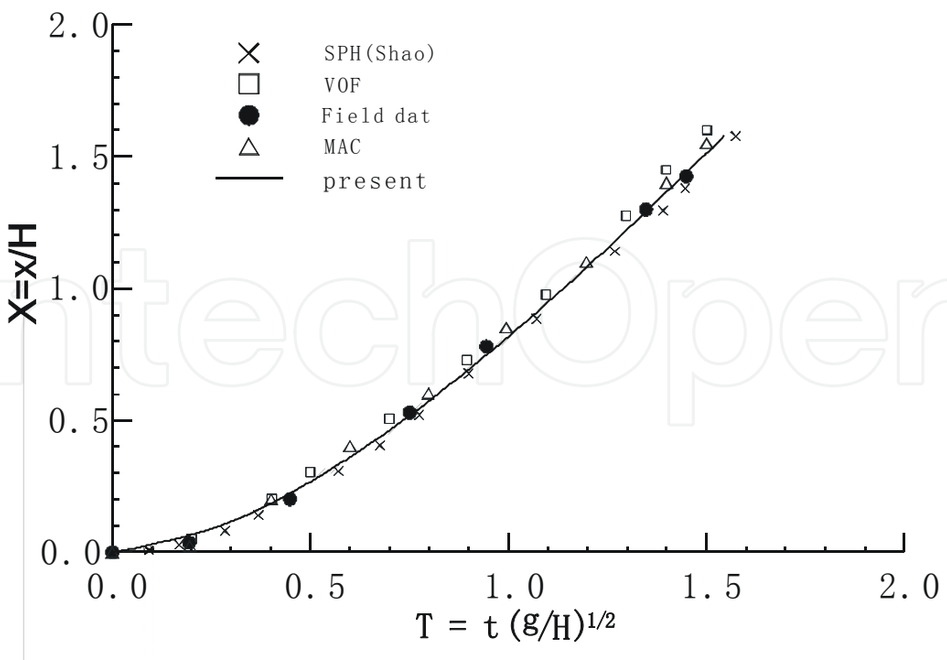

Fig. 5. Relationship between the normalized time T and the leading edge X for dam-breaking flow.

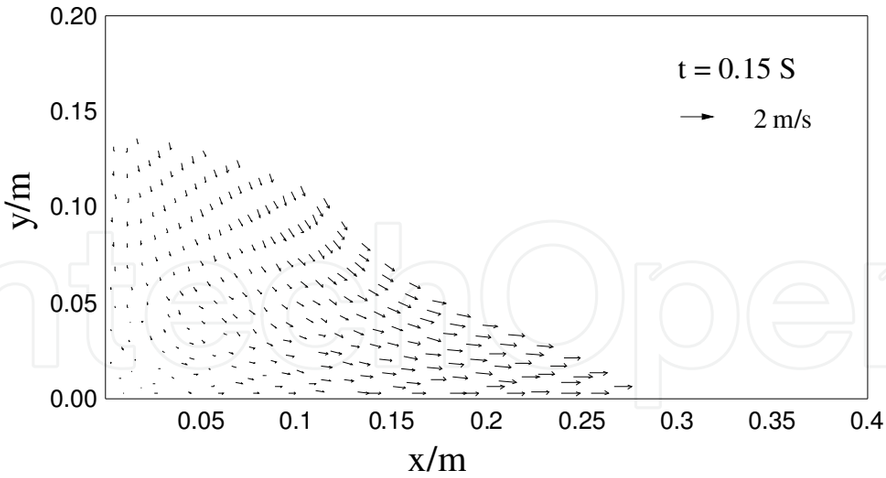

Fig. 6. Velocity field at t = 0.15 s for dam-breaking flow.

3.2 Solitary waves

The transmission of long waves is an important problem in tsunami engineering. Tsunamis can often be simplified as solitary wave or combinations of negative and positive solitary-like waves. In this case, the SPH numerical wave flume is applied to simulate the generation and propagation of a solitary wave with a wave height of 0.018 m over a plane bed. The layout of the flume setup is shown in Figure 7. The flume has a height of 0.2 m and a length of 5 m, which is approximately 4-5 times of the wave length. The initial water depth is 0.1 m. In computation, 80,000 fluid particles are used with an initial spacing of 0.025 m. The smoothing length is 0.006 m. The kinematic viscosity is $\nu = 10^{-6}$ kg·ms^{-1} as the same as in the first case. The propagation of solitary waves during a time scale of 5 s is simulated with a constant time step of 0.0002 s. To reproduce the movement of the experimental wavemaker, the wave-making paddle at the left boundary of tank is represented by a vertical set of particles with prescribed oscillatory frequency and amplitude derived from the first-order solution of the Boussinesq equation[29]

$$\xi = \sqrt{\frac{4Hd}{3}} \tanh\left[\sqrt{\frac{4H}{3d^3}}(ct - \xi)\right] \tag{1.11}$$

where H is the wave height, d the water depth, and c the wave celerity.

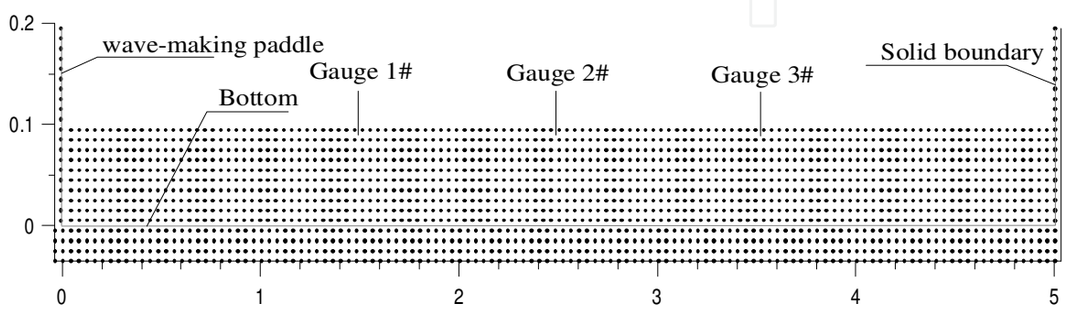

Fig. 7. Layout of numerical wave flume for solitary wave.

The time-evolution of surface elevation at three measuring points x = 1.5m, x = 2.5m and x = 3.5m are collected to verify the numerical results, as shown in Figure 8. The three surface profiles show the good consistency. For each point, the surface elevation remains stationary before wave passing through it and the peak value of surface displays no significant deviation from other two points. That means a stable pressure field is obtained in computation. The observed time lag between two adjacent points is 0.917 s, and the corresponding calculated wave celerity is 1.09 m/s, which agrees well with the analytical value of 1.08 m/s.

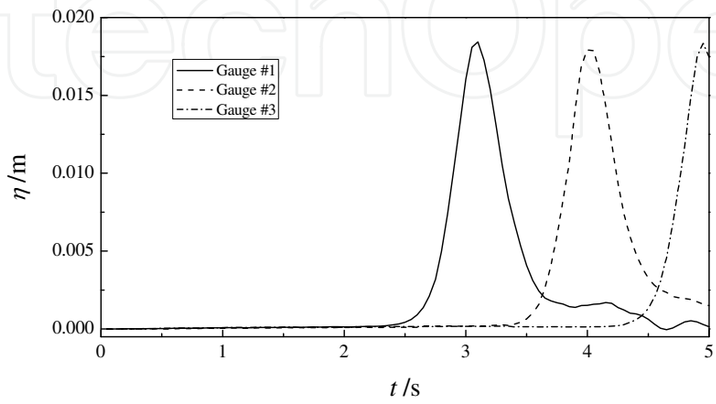

Fig. 8. Time-series of free surface elevation at three measuring points for solitary wave.

Figure 9 presents the simulated free surface at t = 4s, as well as the first-order Boussinesq solution. The overall agreement is satisfactory. The calculated profile is steeper than the theoretical result in front of wave crest while milder behind it, which is due to the kinematic viscosity included in the numerical model but not presented in the analytical solution.

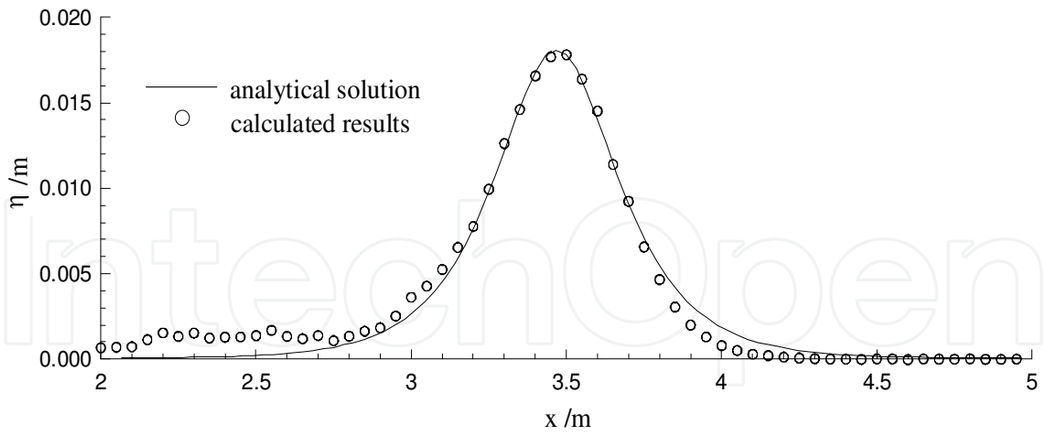

Fig. 9. Free surface variation at t = 4s for solitary wave.

Figure 10 illustrates the velocity field at t = 3s. Realistic result is shown. The horizontal velocity increases with decreasing depth with its peak value locating at the wave crest, where the vertical velocity is negligible. In the water column where wave has passed through, some minor disturbances are found. Nevertheless, generally realistic distributions of both value and direction of velocity are maintained for the whole domain, justifying the ability of the numerical wave flume developed in the present study.

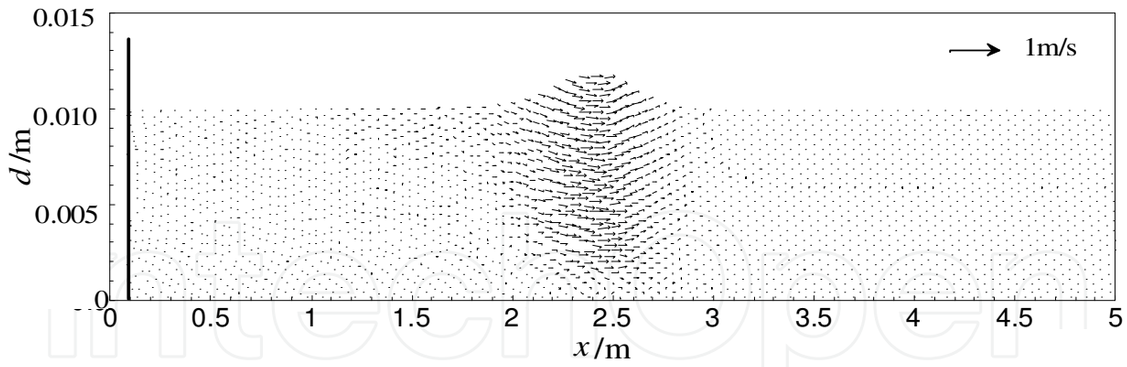

Fig. 10. Velocity field at t = 3 s for solitary wave.

3.3 Regular and irregular waves

The numerical flume has a length of 5 m and a height of 1 m, as well as an initial water depth of 0.65 m, as shown in Figure 11. A 0.9 m high wavemaker is placed at the left boundary of flume to generate irregular waves, and an artificially absorbing sponge layer is configured in the right flume section from 13 m to 16 m. The particle setting in the SPH method is the same as in the case of solitary wave. The time-series of surface elevation are recorded at seven points located at 7.5 m, 8 m, 8.5 m, 9 m, 9.5 m, 10.0 m and 10.5 m along the horizontal axis.

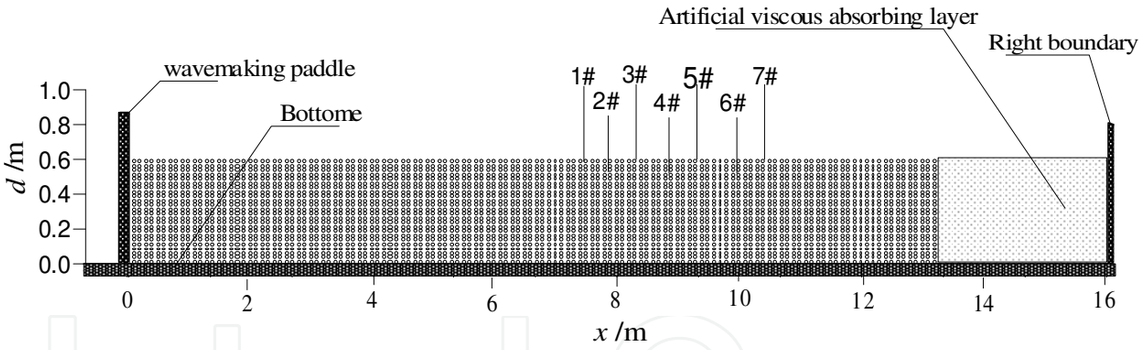

Fig. 11. Layout of numerical wave flume for irregular waves.

3.3.1 Regular waves

For small amplitude waves, it satisfied linearized forms of the kinematic and dynamic free surface boundary conditions, and the shape can be simplified as the sinusoidal form. When wave amplitude increases beyond certain range, the linear wave theory may become inadequate, and the nonlinearity should be considered. Usually, the second-order Stokes wave theory is used to described large amplitude waves, and the wave profile is

$$\eta = \frac{H}{2}\cos(kx-\sigma t) + \frac{H^2 k}{16}\frac{\cosh kh}{\sinh^3 kh}(2+\cosh 2kh)\cos 2(kx-\sigma t) \tag{1.12}$$

where H is height, k is the wave number and σ is the wave angular frequency.

The wave-making paddle at the left boundary oscillates following the method derived by Flick and Guza[30]. Ten successive regular waves with period T = 1s and wave height H = 0.1 m are generated. Figure 12 shows the elevation of the surface at gauges #1, #2, #3 and #4, the line is the second-order Stokes theoretic elevation and the crosses are the results from SPH. Before the first wave reaches the first measurement point, the free surface is not disturbed and keeps stationary, and the wave profile at #1 gets a steady state after 5s. The profile is much more peaked at the crests and flatter at the troughs than the sinusoidal form. Due to the artificial viscosity, the amplitude is decreasing slightly over space. The simulated time lag between #1 and #4 is 0.96s, and the corresponding calculated celerity is 1.60m/s, which is very close to the analytical value 1.54m/s.

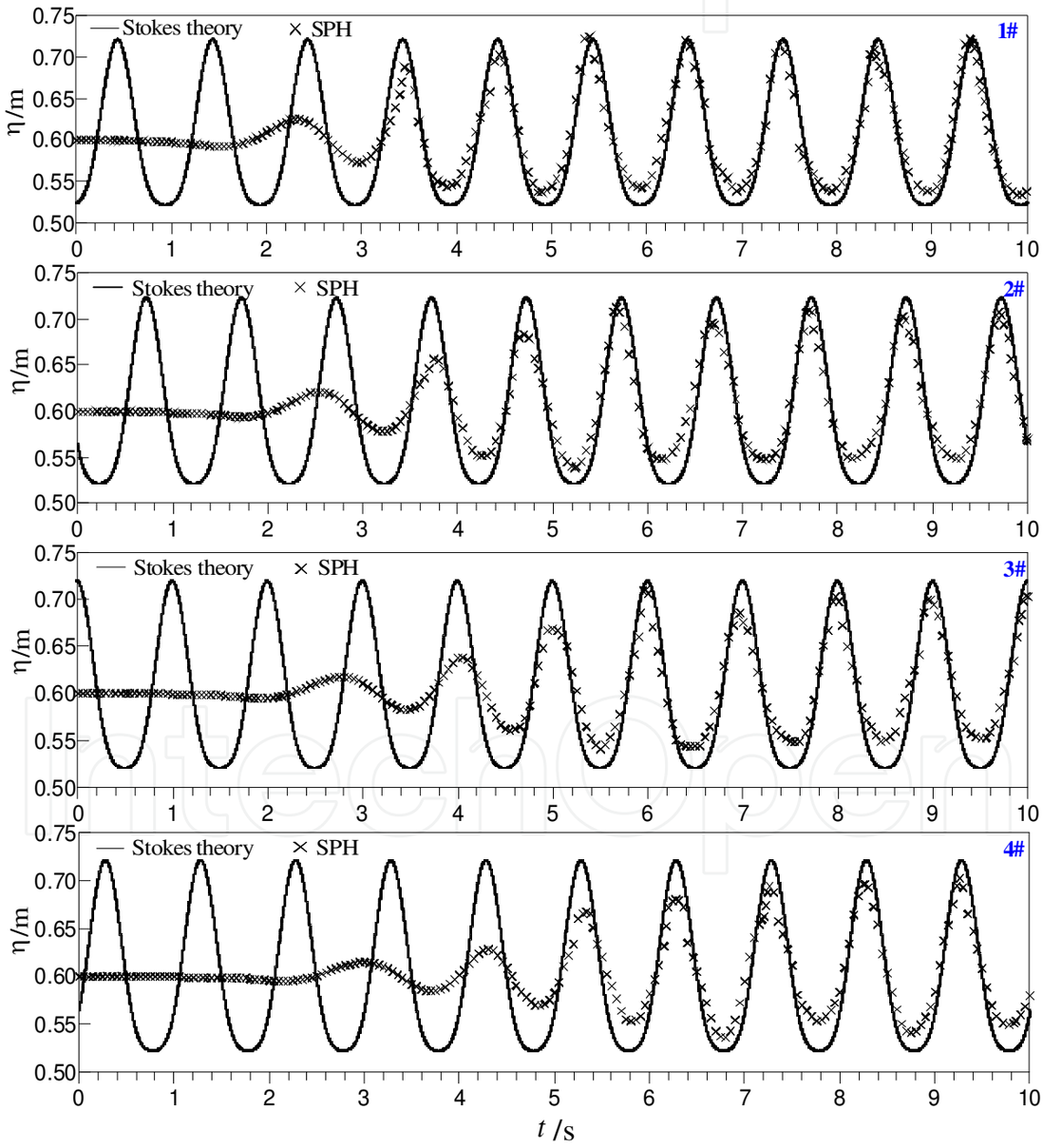

Fig. 12. Comparison of time-series of surface elevation for regular wave generation.

3.3.2 Irregular waves

The wavemaker signal for irregular waves in the experiment of Cox and Ortega[31] is employed in this test. As is shown in Figure 12, it is composed of 4 wave cycles with different frequencies and amplitudes, which gives rise to sharp discontinuities in the transitions between different cycles. These discontinuities will lead to unexpected numerical instabilities. In this study, we follow the approach of Gomez-Gesteira et al.[7], who used a filter function to smooth the signal in the transitions. If the wave-making paddle moves with amplitude A_i and frequency f_i in the interval $t \in [t_i, t_{i+1}]$ with amplitude A_{i+1} and frequency f_{i+1} in the interval $t \in [t_{i+1}, t_{i+2}]$, for any time $t \in [(t_i + t_{i+1})/2, (t_{i+1} + t_{i+2})/2]$, the movement of wavemaker can be described by

$$x(t) = smf_1(t) A_i \sin[f_i(t - t_i)] + smf_2(t) A_{i+1} \sin[f_{i+1}(t - t_{i+1})] \tag{1.13}$$

$$u(t) = smf_1(t) A_i f_i \cos[f_i(t - t_i)] + smf_2(t) A_{i+1} f_{i+1} \cos[f_{i+1}(t - t_{i+1})] \tag{1.14}$$

where smf_1 and smf_2 are smoothing functions expressed as

$$smf_1(t) = 0.5\{-\tanh[(t - t_{i+1}) \cdot \max(f_i + f_{i+1})] + 1\} \tag{1.15}$$

$$smf_2(t) = 0.5\{\tanh[(t - t_{i+1}) \cdot \max(f_i + f_{i+1})] + 1\} \tag{1.16}$$

The smoothed time-series of wavemaker position and velocity are displayed in Figure 13. With this method, a continuous signal is obtained for the numerical experiment.

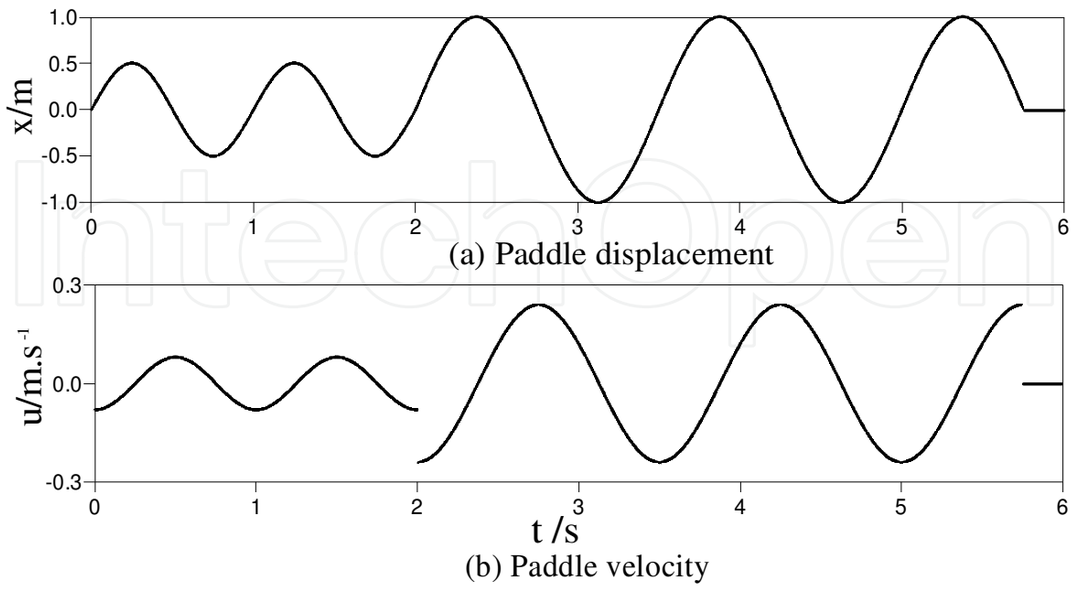

Fig. 13. Original wavemaker signal from Cox and Ortega[31].

Figure 14 presents the comparisons of free surface variations at gauges #1, #2, #3, #4, #5 and #6 between experimental data of Cox and Ortega[31] for the case without a deck, the SPH simulation results from present study and Gomez-Gesteira et al. model[7] (hereafter GGM). The simulated profiles are in generally good agreements with the GGM results and the measurements, both in amplitude and phase, although there are some slight discrepancies between numerical and experimental results for secondary peaks. These discrepancies are probably due to the smoothing effects of wavemaker signal. Particularly for the phase of the first wave and the height of the highest wave, the present model provides fitter results to the observation than GGM's.

Figure 15 shows the particle snapshots in the righter region of flume at t = 11s, t = 13s and t = 15s . The primary aim of this figure is to examine the efficiency of the sponge layer in the model. Waves enter the sponge layer (x =13m ~16m) at t = 13s and begin to dissipate energy in this region. At t = 15s, the surface variation is undistinguishable, indicating that most of wave energy has been effectively absorbed due to the viscous effect in the sponge layer.

It can be reasonably concluded that the SPH numerical wave flume developed in this paper is capable of generating reliable irregular wave trains and reproducing their propagations with good stability and boundary descriptions. Numerical results show the improvements over that of GGM to a reasonable extent. Moreover, only 25 min is needed to complete the computation for this case. This does benefit from the more efficient inner and outer particle searching technique proposed by Zheng et al.[3].

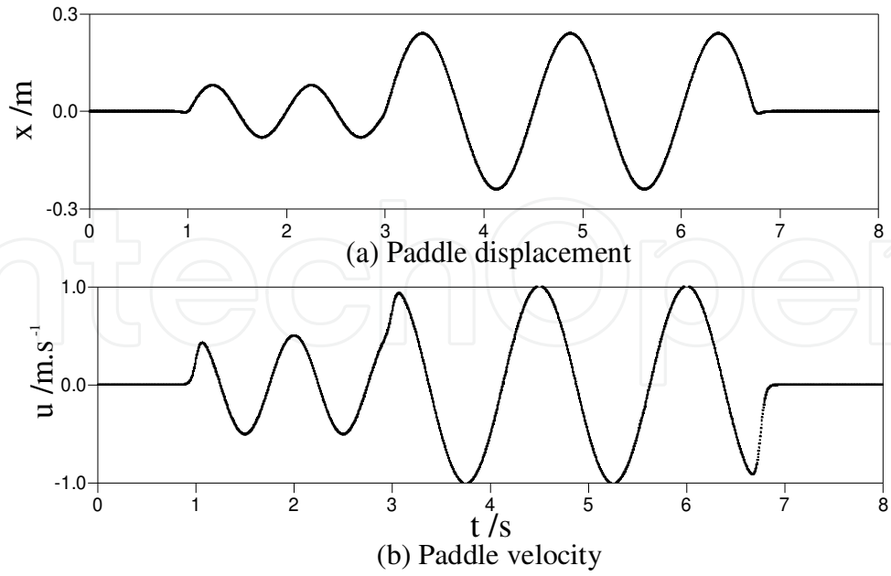

Fig. 14. Wavemaker signal smoothed by the method of Gomez-Gesteira et al.[7].

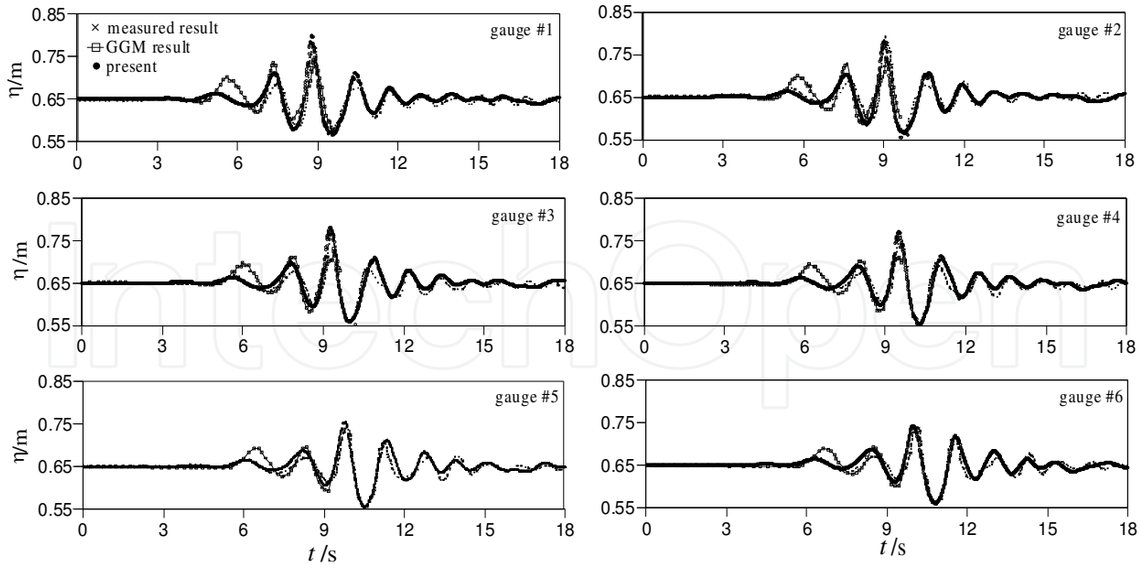

Fig. 15. Comparisons of time-series of surface elevation for irregular wave generation.

4. Application

Since the SPH model has demonstrated an ability to provide numerical solutions to problems such as dam breaking and the generations of solitary waves and irregular waves, this section applies the numerical method for a wide range of solitary wave propagation problems such as the impact of waves on structures, wave run-up and rundown and breaking on a planar slope.

4.1 The run up of a solitary wave on a vertical wall

In many cases, the wave forces on the structure are always related to the structure stability analysis, which in earlier days was mainly made with the use of empirical formulas established on limited number of experimental tests. With the use of SPH method, it is possible to calculate the wave forces on the structure directly. The layout of the flume setup is similar to Figure 7; the length is reduced to 2m to save the calculation time, and the height is increased to 0.3m to prevent the wave running over the wall. Chan and Street [32] have investigated the run-up of solitary waves over the vertical wall by the MAC method and experiments. In order to compare with their results, simulations are carried out with the initial water depth d = 0.2m.

The wave run-up induced by solitary waves with different heights is shown in Figure 16. Clearly, the SPH method yields results that are in excellent agreement with experiments and the MAC method. The run up of a solitary wave on a vertical wall is almost as large as three times of the incident wave height, which is larger than the height of standing waves. Successive stages of wave propagation are shown in Figure 17 and the contour lines of the pressure are shown in Figure 18 for the case H/d = 0.19. Solitary waves propagate keeping a permanent waveform without any breaking. The total pressure is similar to the hydrostatic pressure when solitary waves run up and down.

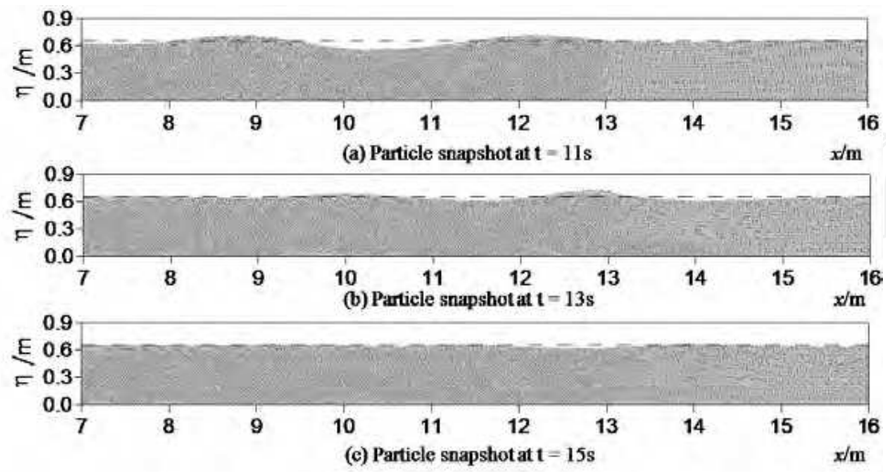

Fig. 16. Particle snapshots for irregular waves.

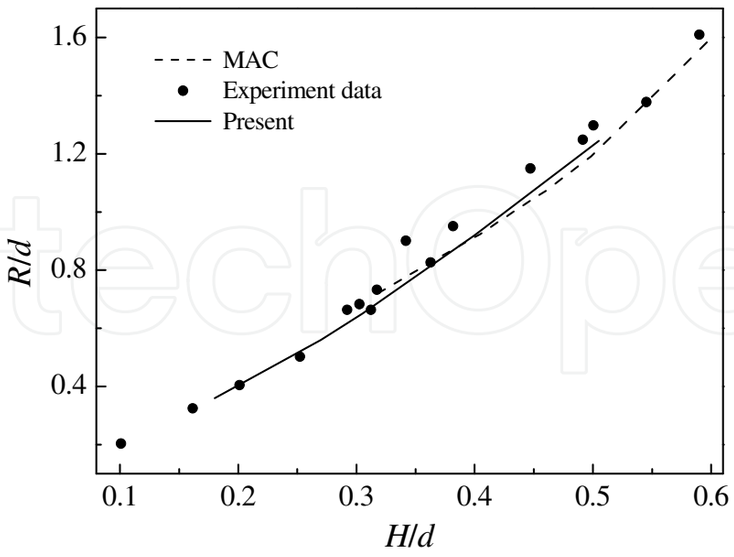

Fig. 17. Wave run up on a vertical wall.

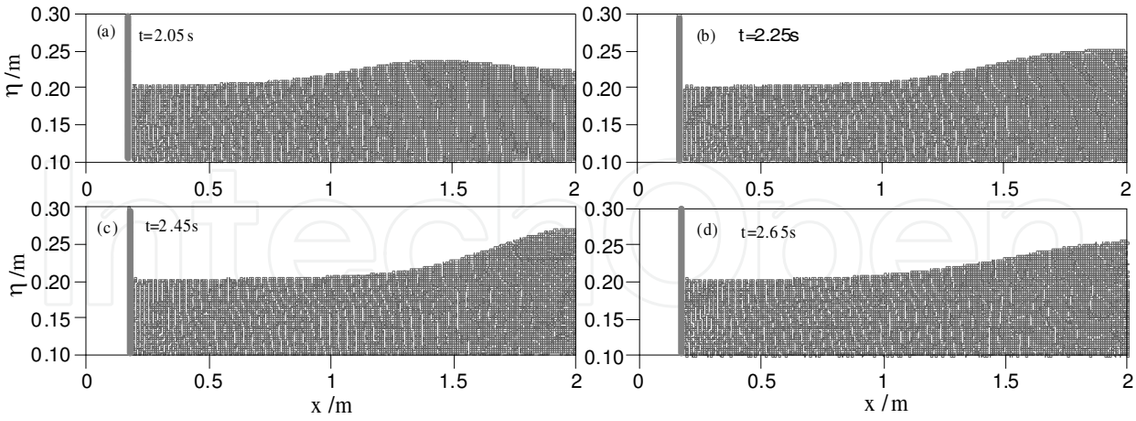

Fig. 18. Particle snapshots for the impact of solitary waves on a vertical wall.

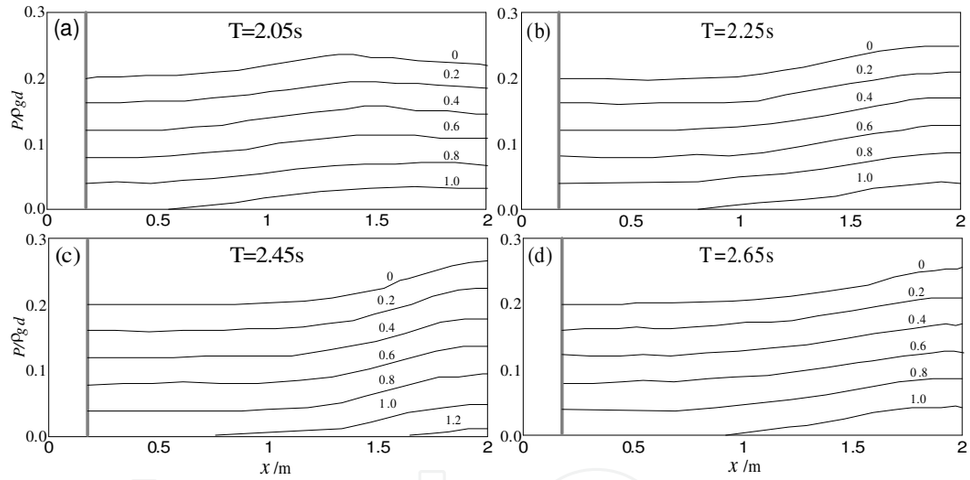

Fig. 19. Pressure distribution.

4.2 Run-up of solitary waves on sloping beaches

The evolution of long waves on a beach is a classic problem in hydrodynamics, and there have been numerous attempts at modeling wave amplification and run-up on sloping beaches. The numerical flume has a length of 8.5m and a height of 0.4m with the initial water depth d = 0.21m, and a beach inclined an angle 2.88^o to the horizontal direction (the slope $s \approx 1/20$) is placed 2m away from the wave-making paddle. A solitary wave with the height of 0.0588m is generated by the paddle following the equation(1.11). Our computational domain represents a 1:10 prototype of Synolakis'[33] experimental setup. In computation, 37,877 fluid particles are used with an initial spacing 0.005m with the smoothing length 0.006m and the kinematic viscosity $\nu = 10^{-6}$m/s^2. A total simulation time of 8s has been considered with an approximate time step of 0.0001s.

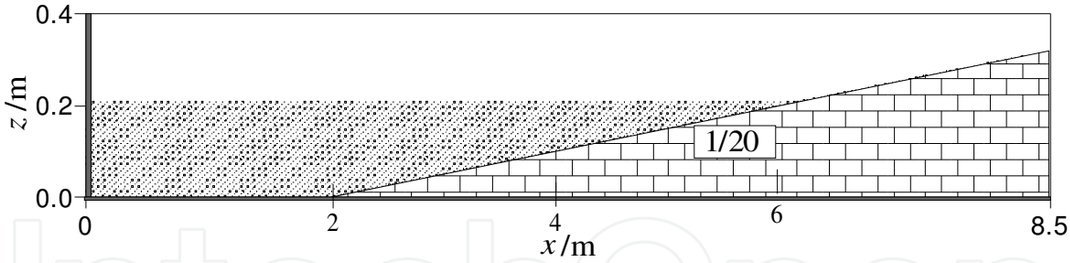

Fig. 20. Layout of numerical flume for run-up of solitary waves on sloping beaches.

The profiles normalized by water depth d versus the normalized time $\tau = t\sqrt{g/d}$ are present in Figure 20. As the wave paddle in the simulation is moved forward to the beach, our results need to be shifted $\Delta\tau$ = 8.958276 to compare with the experiment data. The wave has evolved asymmetric at τ = 15, the front becomes very steep and the height increases to 0.14m much larger than the incident height; The profile becomes vertical and the wave begins to break at τ = 20; the wave has topped over the water below and breaking quickly at τ = 30, then forces the volume to climb up to the beach; the wave runs up to the maximum at τ = 45. Overall, the numerical results and the laboratory data equally well before and after breaking.

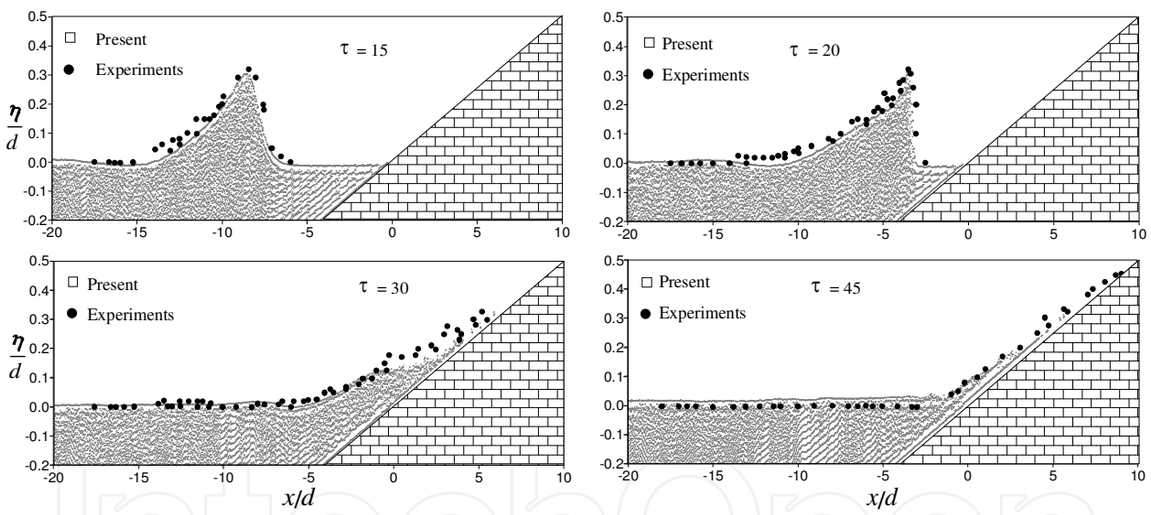

Fig. 21. The clime of a solitary wave with H/d = 0.28 up a 1:20 beach.

5. Conclusions and recommendations

In this paper the application of the SPH method for numerical wave flumes is presented. SPH is a mesh-less method in which particles are used to simulate the fluid. The method has the advantage of solving the governing equations by a Lagrangian approach. By employing an IOPS technique in the SPH simulation, the computation time has been reduced effectively, which improves the method to apply to larger study areas. Several cases are used to investigate its performance, including dam breaking, generation and propagation of solitary wave and irregular wave. Numerical results are in good agreements with theoretical solutions, experimental data and results provided in previous studies. It is concluded that the SPH numerical wave flume with the IOPS method can reproduce the generation and

propagation of realistic waves in a physical tank, which could act as the foundation for further studies involving more complicated flows.

SPH has the potential to replace traditional grid based numerical methods in many applications but more research is needed in order to raise its accuracy and adaptability. Although the IOPS technique has improved the SPH's efficiency, the calculation time is still large especially for a large number of particles. It may be reduced with a more sophisticated interaction find algorithm. Parallelization of the code can also decrease the calculation times significantly. Furthermore, the artificial viscosity keeps the simulation stable, but frequently too dissipative than reality. The improvement of the viscosity model needs further study.

6. References

[1] Gingold, R.A. and Monaghan, J.J., 1977. Smoothed particle hydrodynamics - Theory and application to non-spherical stars. Monthly Notices of the Royal Astronomical Society, 181: 375-389.

[2] Lucy, L.B., 1977. A numerical approach to the testing of the fission hypothesis. Astronomical Journal, 82: 1013-1024.

[3] Zheng, K. et al., 2009. Numerical simulations of water wave dynamics based on SPH methods. Journal of Hydrodynamics, Ser. B, 21(6): 843-850.

[4] Chu, Y. and Lu, W.-q., 2009. Porescale SPH simulation of flow in porous media. Journal of Engineering Thermophysics, 30(3): 437-440.

[5] Ataie-Ashtiani, B. and Shobeyri, G., 2008. Numerical simulation of landslide impulsive waves by incompressible smoothed particle hydrodynamics. International Journal for Numerical Methods in Fluids, 56(2): 209-232.

[6] Xu, Q.-x. and Shen, R.-y., 2008. Fluid-Structure Interaction of Hydrodynamic Damper During the Rush into the Water Channel. Journal of Hydrodynamics, Ser. B, 20(5): 583-590.

[7] Gómez-Gesteira, M., Cerqueiro, D., Crespo, C. and Dalrymple, R.A., 2005. Green water overtopping analyzed with a SPH model. Ocean Engineering, 32(2): 223-238.

[8] Shao, S. et al., 2006. Simulation of wave overtopping by an incompressible SPH model. Coastal Engineering, 53(9): 723-735.

[9] Dalrymple, R.A. and Rogers, B.D., 2006. Numerical modeling of water waves with the SPH method. Coastal Engineering, 53(2-3): 141-147.

[10] Khayyer, A., Gotoh, H. and Shao, S.D., 2008. Corrected Incompressible SPH method for accurate water-surface tracking in breaking waves. Coastal Engineering, 55(3): 236-250.

[11] Gong, K., Liu, H. and Wang, B.-l., 2009. Water entry of a wedge based on SPH model with an improved boundary treatment. Journal of Hydrodynamics, Ser. B, 21(6): 750-757.

[12] SHAO, S., 2005. SPH simulation of solitary wave interaction with a curtain-type breakwater. Journal of Hydraulic Research, 43(4): 366-375.

[13] Gómez-Gesteira, M. and Robert A. Dalrymple, 2004. Using a Three-Dimensional Smoothed Particle Hydrodynamics Method for Wave Impact on a Tall Structure. Journal of Waterway, Port, Coastal, and Ocean Engineering, 130(2): 63-69.

[14] Lv, B., Jin, S. and Ai, C.-f., 2010. A conservative unstructured staggered grid scheme for incompressible Navier-Stokes equations. Journal of Hydrodynamics, Ser. B, 22(2): 173-184.
[15] Christensen, E.D. and Deigaard, R., 2001. Large eddy simulation of breaking waves. Coastal Engineering, 42(1): 53-86.
[16] Zou, L., Lin, Y.-f. and Lam, K., 2008. Large-eddy simulation of flow around cylinder arrays at a subcritical reynolds number. Journal of Hydrodynamics, Ser. B, 20(4): 403-413.
[17] Da-peng, S. and Yu-cheng, L., 2000. Wave damping absorber in numerical wave tank and calculation of wave transformation. China Ocean Engineering, 18(2): 46-50.
[18] Monaghan, J.J., 1985. Particle methods for hydrodynamics. Computer Physics reports, 3(2): 71-124.
[19] Hernquist, L. and Katz, N., 1989. TREESPH - A unification of SPH with the hierarchical tree method. Astrophysical Journal Supplement Series 70: 419-446.
[20] Mihai, B., Marty, L. and Nathan, Q., 2004. Grid-assisted particle search in smoothed particle hydrodynamics, Galway faculty of Engineering Research Day.
[21] Zheng, J.-h., Soe, M.M., Zhang, C. and Hsu, T.-W., 2010. Numerical wave flume with improved smoothed particle hydrodynamics. Journal of Hydrodynamics, Ser. B, 22(6): 773-781.
[22] Liu, G.R. and Liu, M.B., 2003. Smoothed particle hydrodynamics: a meshfree particle method. World Scientific, Singapore, 472 pp.
[23] Koshizuka, S., Nobe, A. and Oka, Y., 1998. Numerical analysis of breaking waves using the moving particle semi-implicit method. International Journal for Numerical Methods in Fluids, 26(7): 751-769.
[24] Violeau, D. and Issa, R., 2007. Numerical modelling of complex turbulent free-surface flows with the SPH method: an overview. International Journal for Numerical Methods in Fluids, 53(2): 277-304.
[25] Harlow, F.H. and Welch, J.E., 1965. Numerical Calculation of Time−Dependent Viscous Incompressible Flow of Fluid with Free Surface Physics of Fluids, 8(12): 2182-2189.
[26] Hirt, C.W. and Nichols, B.D., 1981. Volume of fluid (VOF) method for the dynamics of free boundaries. Journal of Computational Physics, 39(1): 201-225.
[27] Shao, S. and Lo, E.Y.M., 2003. Incompressible SPH method for simulating Newtonian and non-Newtonian flows with a free surface. Advances in Water Resources, 26(7): 787-800.
[28] Martin, J.C. and Moyce, W.J., 1952. Some gravity wave problems in the motion of perfect liquids. Part IV. An Experimental Study of the Collapse of Liquid Columns on a Rigid Horizontal Plane. Philosophical Transactions of the Royal Society of London. Series A, Mathematical and Physical Sciences, 244(882): 312-324.
[29] Synolakis, C.E., 1990. Generation of long waves in laboratory. Journal of Waterway, Port, Coastal and Ocean Engineering, 116(Compendex): 252-266.
[30] Flick, R.E. and Guza, R.T., 1980. Paddle generated waves in laboratory channels. Journal of the Waterway, Port, Coastal and Ocean Division, Proceedings of the American Society of Civil Engineers, 106(Compendex): 79-97.
[31] Cox, D.T. and Ortega, J.A., 2002. Laboratory observations of green water overtopping a fixed deck. Ocean Engineering, 29(14): 1827-1840.

[32] Chan, R.K.C. and Street, R.L., 1970. A computer study of finite-amplitude water waves. Journal of Computational Physics, 6(1): 68-94.
[33] Synolakis, C.E., 1987. The runup of solitary waves. Journal of Fluid Mechanics, 185: 523-545.

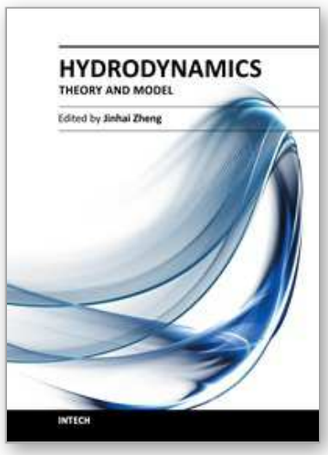

Hydrodynamics - Theory and Model

Edited by Dr. Jin - Hai Zheng

ISBN 978-953-51-0130-7
Hard cover, 306 pages
Publisher InTech
Published online 14, March, 2012
Published in print edition March, 2012

With the amazing advances of scientific research, Hydrodynamics - Theory and Application presents the engineering applications of hydrodynamics from many countries around the world. A wide range of topics are covered in this book, including the theoretical, experimental, and numerical investigations on various subjects related to hydrodynamic problems. The book consists of twelve chapters, each of which is edited separately and deals with a specific topic. The book is intended to be a useful reference to the readers who are working in this field.

How to reference

In order to correctly reference this scholarly work, feel free to copy and paste the following:

Jinhai Zheng, Gang Wang, Chi Zhang and Yingqi Liu (2012). Numerical Wave Flumes Based on Smoothed Particle Hydrodynamics, Hydrodynamics - Theory and Model, Dr. Jin - Hai Zheng (Ed.), ISBN: 978-953-51-0130-7, InTech, Available from: http://www.intechopen.com/books/hydrodynamics-theory-and-model/numerical-wave-flumes-based-on-smoothed-particle-hydrodynamics

INTECH
open science | open minds

InTech Europe
University Campus STeP Ri
Slavka Krautzeka 83/A
51000 Rijeka, Croatia
Phone: +385 (51) 770 447
Fax: +385 (51) 686 166
www.intechopen.com

InTech China
Unit 405, Office Block, Hotel Equatorial Shanghai
No.65, Yan An Road (West), Shanghai, 200040, China
中国上海市延安西路65号上海国际贵都大饭店办公楼405单元
Phone: +86-21-62489820
Fax: +86-21-62489821

IntechOpen